Quadrupolar vibrational mode of silver clusters from plasmon-assisted Raman scattering

B. Palpant
Laboratoire de Spectrométrie Ionique et Moléculaire, CNRS and Université Lyon I, Bâtiment 205, 43 Boulevard du 11 Novembre 1918, 69622 Villeurbanne Cedex, France

H. Portales and L. Saviot
Laboratoire de Physico-Chimie des Matériaux Luminescents, CNRS and Université Lyon I, Bâtiment 205, 43 Boulevard du 11 Novembre 1918, 69622 Villeurbanne Cedex, France

J. Lermé
Laboratoire de Spectrométrie Ionique et Moléculaire, CNRS and Université Lyon I, Bâtiment 205, 43 Boulevard du 11 Novembre 1918, 69622 Villeurbanne Cedex, France

B. Prével
Départment de Physique des Matériaux, CNRS and Université Lyon I, Bâtiment 203, 43 Boulevard du 11 Novembre 1918, 69622 Villeurbanne Cedex, France

M. Pellarin
Laboratoire de Spectrométrie Ionique et Moléculaire, CNRS and Université Lyon I, Bâtiment 205, 43 Boulevard du 11 Novembre 1918, 69622 Villeurbanne Cedex, France

E. Duval
Laboratoire de Physico-Chimie des Matériaux Luminescents, CNRS and Université Lyon I, Bâtiment 205, 43 Boulevard du 11 Novembre 1918, 69622 Villeurbanne Cedex, France

A. Perez
Département de Physique des Matériaux, CNRS and Université Lyon I, Bâtiment 203, 43 Boulevard du 11 Novembre 1918, 69622 Villeurbanne Cedex, France

M. Broyer
Laboratoire de Spectrométrie Ionique et Moléculaire, CNRS and Université Lyon I, Bâtiment 205, 43 Boulevard du 11 Novembre 1918, 69622 Villeurbanne Cedex, France

(Received 8 June 1999)

Absorption and low-frequency Raman-scattering experiments have been performed on thin films consisting of small silver clusters embedded in a porous alumina matrix. When the Raman excitation wavelength is close to the maximum (≈420 nm) of the Mie band (dipolar surface plasmon resonance) the Raman spectra exhibit a strong band located around 10 cm^{-1}, the maximum of which depends on the cluster diameter D at the maximum of the cluster-size distribution in the sample according to the approximate law $\omega_{vib} \propto D^{-1}$. The Raman band corresponds to the excitation of the quadrupolar vibration mode of the clusters, via the plasmon-phonon interaction. Moreover, the maximum of the Raman band shifts towards lower frequencies when the excitation light is shifted to the red. This feature, as well as the rather large Mie-band width, is shown to reflect the ellipsoidal shape distribution of part of the embedded clusters. [S0163-1829(99)02048-2]

I. INTRODUCTION

Nanocrystals are currently attracting much interest because their physical properties differ strongly from those of the bulk phase. In particular, their specific optical properties, that stem from the conduction electron confinement and the large surface-to-volume ratio, have been extensively studied both experimentally and theoretically,[1–3] and may find important applications in optical devices. The effect of confinement on the vibration modes (phonons) and the electron-phonon coupling, which are known to be important factors in determining the dynamical processes in bulk materials (transport, inelastic electron scattering, etc.), are comparatively much less documented. In particular, only very few experimental works are concerned with Raman scattering from confined acoustic phonons in matrix-embedded nanoparticles.[4–7] Information about the electron-phonon coupling obtained through such experiments would be of particular relevance for cluster physics. Previous experimental studies have pointed out that reliable interpretation of Raman spectra requires characterization, as complete as possible, of the nanostructured composite samples which usually involve both large cluster-size and -shape distributions.[8] Therefore, the Raman spectra reported in this paper (Sec. III) are analyzed against relevant characterization experiments, as for

instance, optical absorption (Sec. III) and transmission electron microscopy (TEM) (Sec. II). The qualitative consistency of the whole results we obtained on Ag_N : alumina samples is emphasized in the discussion (Sec. IV). This suggests that quantitative data about the vibration modes and the electron-phonon coupling in nanosized clusters could be deduced from Raman-scattering experiments, allowing to test the available theoretical models.

II. SAMPLE PRODUCTION AND CHARACTERIZATION

Silver clusters are produced by laser vaporization and the composite Ag_N : alumina films by a low-energy cluster beam deposition technique.[9] The hot atomic plasma, created by the impact of a pulsed Nd-Yag laser (~10 Hz) onto a silver rod, is thermalized by helium gas, leading to cluster growth. Clusters are then quenched during a supersonic expansion at the exit of the source chamber. The neutral Ag_N clusters are deposited simultaneously with the alumina matrix (evaporated continuously by electron bombardment) on different substrates at room temperature. The size distribution of the embedded clusters can be varied by modifying the helium gas pressure. Two quartz balances allow to measure and adjust the cluster and matrix deposition rates, and therefore to control both the total film thickness and the volumic fraction of metal (a few percent for each sample). The film thickness is about 250 nm for low-frequency Raman scattering and absorption measurements, and about 15 nm for TEM.

Direct thickness measurements by alpha step, as well as ellipsometric fits, reveal a porosity of the amorphous alumina matrix of about 45% with respect to crystalline Al_2O_3. Rutherford backscattering experiments provide depth profiles and atomic concentrations. Results on a pure alumina film show a slight overstoichiometry according to the formula $Al_2O_{3,2}$. TEM, performed on the different samples, shows that most clusters are roughly spherical and randomly distributed in the matrix. A small, but noticeable amount of clusters—generally the largest ones—have a prolate ellipsoidal shape, resulting probably from the initial random stacking and the partial coalescence following diffusion during the film growth. The size distributions are deduced from the TEM micrographs over a population of 700 up to 3000 particles, depending on the sample. The mean diameter of silver particles ranges from 3.1 to 7.1 nm. X-ray diffraction and diffusion experiments performed at the LURE facility (Orsay, France) reveal a fcc structure and confirm the mean size of the clusters deduced from TEM.

III. ABSORPTION AND RAMAN-SCATTERING EXPERIMENTS

Absorption measurements are performed on Ag_N : alumina films deposited on suprasil substrates with a Varian double-beam spectrophotometer, over a wavelength domain 200—1000 nm. Results of absorption versus energy for different cluster size distributions are displayed in Fig. 1. For each sample, one observes an absorption band (Mie resonance) located around 2.9 eV. This band reflects the surface plasmon resonance corresponding to the collective oscillation of the conduction electrons with respect to the ionic background. The location of the Mie band is nearly size independent. This quenching of the size effects in the optical absorption of Ag_N clusters is partly due to the energy dependence of the dielectric function corresponding to the *d* electrons.[10] Let us recall that interband transitions (valence *d* band→conduction hybridized *sp* band) occur at higher energies and only the onset is observed in the displayed energy domain. The bandwidth is rather large and is thought to reflect mainly both the cluster-shape distribution and the cluster dependence of the local porosity at the metal/matrix interface.[10] The slight increase of the bandwidth as the mean diameter increases (seemingly inconsistent with the well-known limited-mean-free-path model[11]) is due to the fact that the distortion from the spherical shape is more frequent and pronounced for large embedded nanoparticles (observed in TEM). These assumptions are quite consistent with the wavelength dependence of the Raman spectra (see Sec. IV).

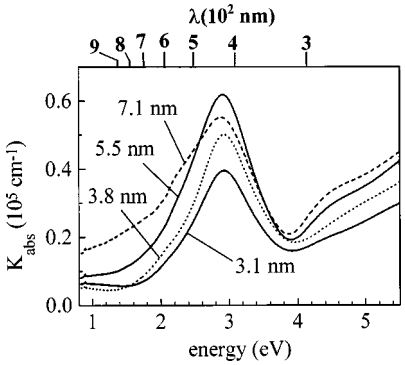

FIG. 1. Absorption coefficient as a function of the photon energy recorded for four different composite Ag_N :alumina samples. The mean diameter $\langle D \rangle$ of the cluster-size distribution is indicated for each sample.

The Raman spectra are recorded on a DILOR Z40 monochromator. The high rejection rate of this setup, which is due to its five gratings, makes it possible to measure a low-frequency Raman signal close to the Rayleigh line. All the visible lines of an Ar^+ and a Kr^+ laser [wavelength ranging from 406.7 nm (3.05 eV) to 676.4 nm (1.83 eV)] are used for excitation. The excitation power is close to 30 mW. It is controlled that the laser beam does not heat the sample. Measurements at low temperature in a cryostat (down to 10 K) shows that the Stokes/anti-Stokes ratio corresponds to the measured temperature of the sample holder. The incoming light beam is at grazing incidence and the scattered one is detected at $\pi/2$ with respect to excitation. Two different configurations are employed, with the excitation and detection polarizations either parallel (VV) or perpendicular (VH) to each other. To obtain a depolarization ratio, I_{VH}/I_{VV}, independent of the excitation conditions, a half-wavelength plate, which rotates the polarization of the scattered light of an angle equal to 0 or $\pi/2$, and a polarizer, which filters the V component of the light, are placed in front of the spectrometer to select, respectively, the V or H component of the scattered light. Low-frequency Raman spectra are displayed in Fig. 2 for four cluster-size distributions (excitation energy below but close to the Mie-band maximum). A well-defined peak around 10 cm^{-1}, evolving qualitatively according to Lamb's theory for the acoustic vibration modes,[12] namely, $\omega_{vib} \propto D^{-1}$, is observed. As for the Mie band in the case of light absorption, the rather large peak width reflects the

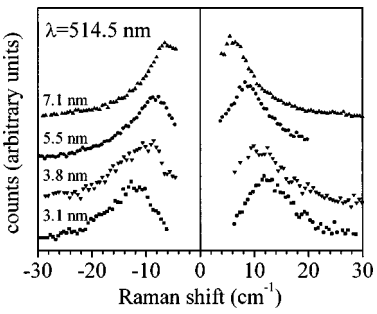

FIG. 2. Room-temperature Raman-scattering spectra recorded for the four samples involved in Fig. 1, under 514.5-nm excitation (2.41 eV). The various curves have been vertically shifted and independently scaled for clarity.

cluster-size and -shape distributions in the various samples. Figure 3 shows Raman spectra recorded at various excitation lines in the case of a sample characterized by the mean diameter $\langle D \rangle = 3.8$ nm. The most striking change versus the excitation wavelength is the steady Raman peak shift towards the Rayleigh line when the excitation energy is progressively lowered. The I_{VH}/I_{VV} depolarization ratio, which is measured, decreases with the wavelength of the incident light as shown in Table I.

The absolute scales of the various Raman spectra displayed in Figs. 2 and 3 cannot be quantitatively compared because the recorded signal depends on numerous experimental factors. Normalization by the laser fluence and the integration time can be easily taken into account. However, the signal depends also critically on the laser spot area onto the sample and the tilting of the surface relative to both the incoming light (grazing incidence) and the detected scattered light (normal to the surface). Moreover, the signal depends on the metal concentration, and the local concentration in the zone involved in the Raman experiment may differ from the average and local estimates deduced from, respectively, the quartz balance and Rutherford backscattering measurements. Therefore each Raman spectrum has been independently scaled for clarity in both figures.

IV. DISCUSSION

As will be discussed in this section, the results of the Raman-scattering experiments are full consistent with the other characterization methods, and, moreover, provide strong support to some assumptions concerning the morphology at the metal/matrix interface and the partly inhomogeneous nature of the Mie resonance broadening.

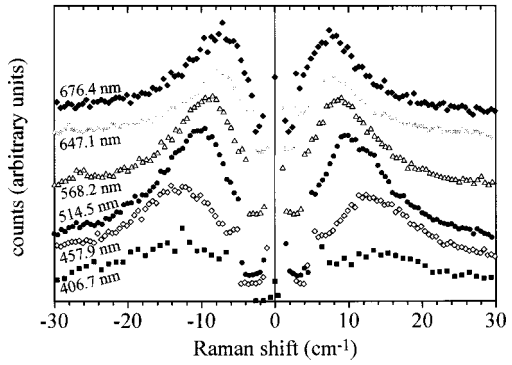

FIG. 3. Laser-wavelength dependence of the low-frequency Raman-scattering spectrum. The displayed spectra have been recorded from the $\langle D \rangle = 3.8$-nm sample. The various curves have been vertically shifted and independently scaled for clarity.

TABLE I. Depolarization ratio ($I_{VH}I_{VV}$) for two composite Ag_N alumina samples. D_{max} is the diameter corresponding to the maximum of the cluster-size distribution, and ω_{max} is the position of the maximum of the low-frequency Raman scattering.

Laser wavelength (nm)	D_{max} (nm)	ω_{max} (cm^{-1})	$\frac{I_{VH}}{I_{VV}}$
457.9	3.0	11.9	0.61
	3.45	11.2	0.59
514.5	3.0	10.0	0.51
	3.45	8.8	0.58
647.1	3.0	8.2	0.37
	3.45	7.3	0.38

The acoustic vibration modes of the nanoparticles, determined from the Raman spectra, reflect their size and shape symmetry. Since the mean radius of the crystallized clusters exceeds 1 nm, the vibration modes can be estimated, in a first approximation, by assuming that the medium inside the particle is homogeneous and isotropic.[12,13] For a sphere the modes are characterized by the quantum numbers l and m (as for the spherical harmonic functions related to the symmetry group of the sphere) and the index $n \geqslant 1$ labeling—in increasing order of frequency—the sequence of the eigenmodes for given l and m values ($2l+1$ degeneracy of the l modes). Among the two types of modes, i.e., torsional (only shear motion) and spheroidal (shear and stretching motions), it was theoretically shown by group theory that only the $l=0$ and 2 spheroidal modes can Raman scatter the light.[14] The probability of scattering by the different modes $l=0$, $l=2$, depends on the Raman-scattering process. For a cubic lattice and a dipole-induced dipole mechanism of light scattering, it was predicted that the $l=0$ mode is not Raman active and the quadrupolar surface modes ($l=2$, $n=1$) dominate by far the Raman process. These predictions of quadrupolar modes observation by Raman scattering are supported by previous experiments,[5,7] and are consistent with our presented Raman spectra. However, with such a mechanism, a depolarization ratio, I_{VH}/I_{VV}, was determined to be equal to 1/3.[15] This value is at variance with our measurements, in particular by excitation in the blue and the green.

The Raman scattering is observed when the light excites the dipolar surface plasmon, which corresponds to a big oscillating electric dipole. It means that an effect of resonance occurs. In this case the inelastic light scattering is induced by the plasmon-phonon coupling, which creates (Stokes scattering) or annihilates (anti-Stokes scattering) one phonon. As noted earlier by Gersten *et al.*,[8] it is not expected that a spherical vibrational oscillation ($l=0$ mode) will produce significant modulation of the electric dipole. In consequence, the Raman scattering by $l=0$ mode will be very low if visible. Conversely, the quadrupolar or ellipsoidal distortions are strongly coupled to the dipolar plasmon,[8] so that the Raman scattering of the $l=2$ modes is strongly enhanced by plasmon resonance. The polarization of the Raman transi-

tions for the different $l=2$ modes ($m=\pm 2, \pm 1, 0$) in spherical symmetry were determined by Mariotto *et al.*:[5] a depolarization ratio of 0.75 is obtained.

If the cluster is ellipsoidally distorted and has a prolate shape, the threefold degenerate $L=1$ dipolar plasmon is split to give a lower-energy nondegenerate plasmon, which corresponds to a dipole oscillating along the long axis, and a higher-energy twofold degenerate plasmon with a dipole oscillating in the plane perpendicular to the long axis. A distribution of ellipsoidal distorsions of silver clusters explains the observed large inhomogeneous width of the plasmon absorption, as the plasmon energy is very weakly dependent on size.[10] The ellipsoidal distorsion lifts also the fivefold degeneracy of the vibrational $l=2$ modes, and for a prolate shape, the lowest-frequency nondegenerate oscillation is along the ellipsoid long axis.

As the absorption has a maximum at 420 nm, when we use the 457.9-nm argon line, we excite principally the spherical clusters and a depolarization ratio close to 0.75 would be expected. By excitation with the krypton red lines, 647.1 or 676.4 nm, in the low-energy wing of the absorption band, which is due to the ellipsoidal clusters, the Raman scattering from the lowest-frequency nondegenerate vibrational mode is predicted to be strongly enhanced. There are two reasons for this strong enhancement: (1) absorption increases with the amplitude of the ellipsoidal distorsion,[8,16] through the excitation of the lowest-energy nondegenerate plasmon of prolate clusters; and (2) for the same reason that the nondegenerate plasmon is strongly coupled to the static distorsion along the long axis, the nondegenerate vibrational mode, involving atoms moving along the long axis, is strongly coupled to the nondegenerate plasmon. This plasmon is precisely excited in the red. The selection rules for the creation or the annihilation of one phonon by phonon-plasmon coupling is simply deduced from group theory. From this, it is clear that the creation (annihilation) of one phonon in the nondegenerate mode comes from the coupling of vibration with the nondegenerate plasmon. Because the electric dipole corresponding to the nondegenerate plasmon oscillates along the ellipsoid long axis the polarization of the enhanced field inside the cluster (the primary field for the Raman process) and of the scattered light will be parallel to this long axis. With the reasonable hypothesis that the ellipsoidal clusters are randomly oriented, after angular averaging, a depolarization ratio equal to 1/3 is obtained.

Going from ellipsoidal clusters to spherical ones the depolarization ratio, I_{VH}/I_{VV}, varies from 0.33 to 0.75 according to theory. Experimentally, from the red to the blue excitations, I_{VH}/I_{VV} goes from 0.37 to 0.61 (see Table I). Knowing that at 457.9 nm we excite spherical clusters, but also, in a small proportion, ellipsoidal ones, the experimental situation corresponds very well to the above described one. On the other hand, we excite mainly the ellipsoidal clusters by excitation at 647.1 and 676.4 nm. Besides, from the dependence on eccentricity (the ratio of both half axes of the ellipsoid) of the plasmon energies and of the vibration frequencies,[8] it is estimated that the eccentricity of the clusters excited in the red is around 2. It can be due to the coalescence of two smaller silver nanoclusters. At this point of the discussion, and before examining the cluster-size dependence of the Raman intensity, it would be noticed that the present analysis has to do with the theoretical work of Kerker, Siiman, and Wang,[17] in which it is stated that a strong redshifted surface enhanced Raman scattering (SERS) of molecules, which are adsorbed on silver, may occur in the presence of a very small fraction of nonspherical particles, even when their amount is unsufficient to give a significant shoulder on the extinction spectrum at the corresponding wavelength. Indeed, by excitation in the red, an electric dipole oscillating along the long axis of the ellipsoid is created, which induces a very strong external field close to the tip of the nanocluster.

The frequency dependence of the Raman intensity for the Stokes component is generally expressed as follows:[18]

$$I(\omega)=\frac{n(\omega)+1}{\omega}\sum_i g_i(\omega)C_i(\omega), \tag{1}$$

where $n(\omega)$ is the Bose factor, $g_i(\omega)$ and $C_i(\omega)$ are, respectively, the density of vibrational modes and the light-vibration coupling coefficient for the modes of type i. It is interesting to examine $I(\omega)$, obtained with the 457.9-nm laser line, which excites mainly the spherical clusters. From above only the quadrupolar modes scatter the light, so that the relation between frequency and cluster size is given by[5,12]

$$\omega(\mathrm{cm}^{-1})=\frac{0.85}{c}\frac{v_t}{D(\mathrm{cm})}, \tag{2}$$

where v_t is the transverse sound velocity in the silver particles. Assuming that the structure of silver in clusters is close to the macroscopic one, $v_t \approx 1660$ m/s, and, consequently,

$$\omega(\mathrm{cm}^{-1})\approx\frac{47}{D(\mathrm{nm})}. \tag{3}$$

The density of vibrational modes, $g(\omega)$, is such that $g(\omega)d\omega$ is equal to the number of the clusters that oscillate ellipsoidally between ω and $\omega+d\omega$. Consequently, $g(\omega)d\omega=F(D)dD$, $F(D)$ being the cluster diameter distribution. At low energy and room temperature, $n(\omega)+1 \approx kT/\hbar\omega$, therefore,

$$I(\omega)\propto\omega^{-2}C(\omega)g(\omega), \tag{4}$$

and one obtains the following scaling:

$$\frac{I(\omega)}{C(\omega)}\omega^4\propto F(D). \tag{5}$$

From this scaling, the diameter, $D_{\max}$, at the maximum of the $F(D)$ experimental distribution, is related to the maximum, $\omega_{\max}$ of $[I(\omega)/C(\omega)]\omega^4$ through Eq. (3). The best straight line, $\omega_{\max}=A(D_{\max})^{-1}$, is obtained for $I(\omega)\propto F(D)$, with $A\approx 36$ (Fig. 4). This value is not far from 47, as in Eq. (3). It means that $C(\omega)\propto\omega^4$. This scaling cannot be obtained from the different processes of nonresonant Raman scattering,[15,19] for which the maximum value of the ω exponent in $C(\omega)$ is 2. It is likely that such a scaling comes from the resonance with the plasmon excitation and the plasmon-phonon coupling. A theoretical study of this resonant Raman scattering is now in progress.

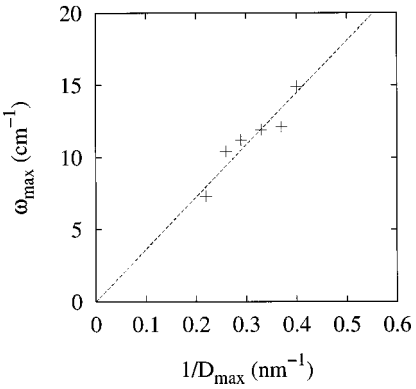

FIG. 4. Plot of the frequency (ω_{max}) at the maximum of the Raman intensity against the inverse of diameter (D_{max}) at the maximum of the cluster-size distribution.

V. CONCLUSION

This experimental study confirms that low-frequency Raman scattering from silver nanoclusters comes from the quadrupolar modes. This selection of modes by Raman scattering is due to the stronger plasmon-phonon coupling for these modes. The resonance Raman scattering selects not only the type of modes, but also the shape of clusters, as shown by the light polarization analysis. By excitation in the blue, close to the absorption maximum, one observes the spherical nanoclusters. By shifting more and more the excitation to the red, one observe clusters which are more and more ellipsoidally distorted. This is due to the splitting of the dipolar plasmon by the ellipsoidal distorsion, and the shift to the red of the ($L=1$, $m=0$) resulting nondegenerate plasmon, which is strongly coupled to the ($l=2$, $m=0$) nondegenerate vibrational mode. In addition to the shape selection by the wavelength of the laser excitation, it is indicated that the width of the plasmon absorption is inhomogeneous and due to the cluster-shape distribution. Even if the mechanism of SERS is different from the one of low-frequency Raman scattering by cluster vibrations, the surface enhancement scattering and the relatively strong low-frequency scattering have at least a common cause. This is the effect of resonance with the excitation of oscillating electric dipoles, which have an axial symmetry. Such an excitation has a good rate in the red spectral range. The dependence of the Raman intensity on frequency, or on cluster size, which confirms the resonant character of the low-frequency Raman scattering, will allow to establish a quantitative model of the plasmon-phonon coupling and of the resonant Raman scattering from metallic nanoclusters.

[1] W. A. de Heer, Rev. Mod. Phys. **65**, 611 (1993).
[2] M. Brack, Rev. Mod. Phys. **65**, 677 (1993).
[3] U. Kreibig and M. Vollmer, *Optical Properties of Metal Clusters* (Springer, New York, 1995).
[4] E. Duval, A. Boukenter, and B. Champagnon, Phys. Rev. Lett. **56**, 2052 (1986).
[5] G. Mariotto, M. Montagna, G. Viliani, E. Duval, S. Lefrant, E. Rzepka, and C. Maï, Europhys. Lett. **6**, 239 (1988).
[6] M. Fujii, T. Nagareda, S. Hayashi, and K. Yamamoto, Phys. Rev. B **44**, 6243 (1991).
[7] M. Ferrari, L. M. Gratton, A. Maddalena, M. Montagna, and C. Tosello, J. Non-Cryst. Solids **191**, 101 (1995).
[8] J. I. Gersten, D. A. Weitz, T. J. Gramila, and A. Z. Genack, Phys. Rev. B **22**, 4562 (1980).
[9] A. Perez, P. Mélinon, V. Dupuis, P. Jensen, B. Prével, J. Tuaillon, L. Bardotti, C. Martet, M. Treilleux, M. Broyer, M. Pellarin, J. L. Vialle, B. Palpant, and J. Lermé, J. Phys. D **30**, 709 (1997).
[10] J. Lermé, B. Palpant, B. Prével, M. Pellarin, M. Treilleux, J. L. Vialle, A. Perez, and M. Broyer, Phys. Rev. Lett. **80**, 5105 (1998).
[11] H. Hövel, S. Fritz, A. Hilger, U. Kreibig, and M. Vollmer, Phys. Rev. B **48**, 18 178 (1993).
[12] H. Lamb, Proc. London Math. Soc. **13**, 187 (1882).
[13] A. Tamura, K. Higeta, and T. Ichinokawa, J. Phys. C **15**, 4975 (1982).
[14] E. Duval, Phys. Rev. B **46**, 5795 (1992).
[15] M. Montagna and R. Dusi, Phys. Rev. B **52**, 10 080 (1995).
[16] A. Berger, J. Non-Cryst. Solids **163**, 185 (1993).
[17] M. Kerker, O. Siiman, and D. S. Wang, J. Phys. Chem. **88**, 3168 (1984).
[18] R. Shuker and R. W. Gammon, Phys. Rev. Lett. **25**, 222 (1970).
[19] E. Duval, N. Garcia, A. Boukenter, and J. Serughetti, J. Chem. Phys. **99**, 2040 (1993).